NANO LETTERS

pubs.acs.org/NanoLett Letter

Control over Charge Carrier Mobility in the Hole Transport Layer Enables Fast Colloidal Quantum Dot Infrared Photodetectors

Ozan Atan, Joao M. Pina, Darshan H. Parmar, Pan Xia, Yangning Zhang, Ahmet Gulsaran, Eui Dae Jung, Dongsun Choi, Muhammad Imran, Mustafa Yavuz, Sjoerd Hoogland, and Edward H. Sargent*

Cite This: https://doi.org/10.1021/acs.nanolett.3c00491 Read Online

ACCESS | Metrics & More | Article Recommendations | Supporting Information

ABSTRACT: Solution-processed colloidal quantum dots (CQDs) are promising materials for photodetectors operating in the short-wavelength infrared region (SWIR). Devices typically rely on CQD-based hole transport layers (HTL), such as CQDs treated using 1,2-ethanedithiol. Herein, we find that these HTL materials exhibit low carrier mobility, limiting the photodiode response speed. We develop instead inverted (p-i-n) SWIR photodetectors operating at 1370 nm, employing NiOx as the HTL, ultimately enabling 4× shorter fall times in photodiodes (~800 ns for EDT and ~200 ns for NiOx). Optoelectronic simulations reveal that the high carrier mobility of NiOx enhances the electric field in the active layer, decreasing the overall transport time and increasing photodetector response time.

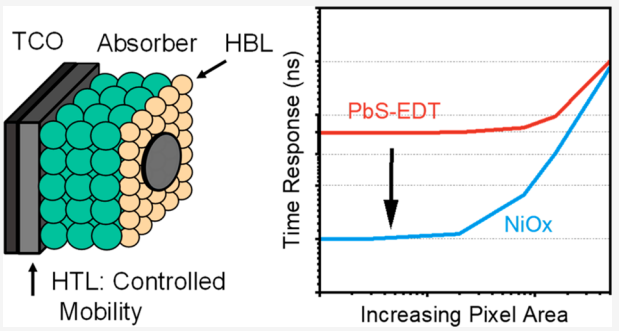

KEYWORDS: *quantum dots, infrared, photodetectors, carrier mobility, time-of-flight*

Short-wave infrared (SWIR) photodetectors are used in applications including medical imaging, biometric authentication, machine vision, spectroscopy, and depth estimation.[1−4] Depth estimation techniques such as time-of-flight and structured light are of interest for autonomous driving and augmented reality.[5,6] These systems rely on the temporal detection of reflected or scattered light from the observed scene; thus, they must detect low photon fluxes at high speeds.[7]

Commercial depth imaging detectors commonly use silicon (Si) photodetectors; however, these detectors are limited to wavelengths shorter than 1100 nm.[2,8] At these wavelengths, background illumination—in particular, sunlight—contributes to background current, and this hinders the ability to pick out the signal from the high background.[2,9,10] Operating at 1370 nm reduces background interference in view of the reduced solar intensity in this spectral band (Figure S1).

Colloidal quantum dot (CQDs) can be synthesized to absorb to 1370 nm light. CQDs are semiconductors having tunable electronic and optical properties, with bandgaps from the visible to the infrared.[11,12] PbS CQDs benefit from facile solution processing, allowing integration with Si read-out integrated circuits (ROICs).[13]

The active layer in PbS CQD photodetectors has seen much focus and major advances as a result.[2,3,5] These efforts have enabled highly efficient PbS CQD photodetectors with a low dark current and high external quantum efficiency (EQE). However, an additional important photodetector figure of merit is speed. PbS CQD photodetectors have shown promising performance in dark current and EQE compared to Si and InGaAs; however, their speed performance is considerably lower than in these traditional technologies. It is of interest to deepen the understanding of the charge transport processes in CQD photodetectors, including the influence of charge transport layers, and to enhance speed.

We investigate herein the temporal response of conventional photodiodes using experimental and theoretical tools (electrical and optical characterization). We developed first a model to study how the electric field is distributed in PbS CQD photodetectors. We found that increasing the carrier mobility of the charge carriers in the transport layers is crucial to achieving faster temporal response.

This motivated us to replace the HTL typically used in prior PbS CQD photodetectors, ethane-1,2-dithiol (EDT) treated PbS CQDs, with a higher-mobility HTL, NiOx. We demonstrated that NiOx decreases the fall time of the detector 4× compared to EDT.

To investigate the temporal response of PbS CQD photodetectors, we fabricated p-i-n devices operating at 1370 nm based on prior approaches.[2,3] The structure of this device is shown in Figure 1a. Two different sizes of oleic acid capped

Received: February 7, 2023
Revised: May 5, 2023

https://doi.org/10.1021/acs.nanolett.3c00491
Nano Lett. XXXX, XXX, XXX−XXX

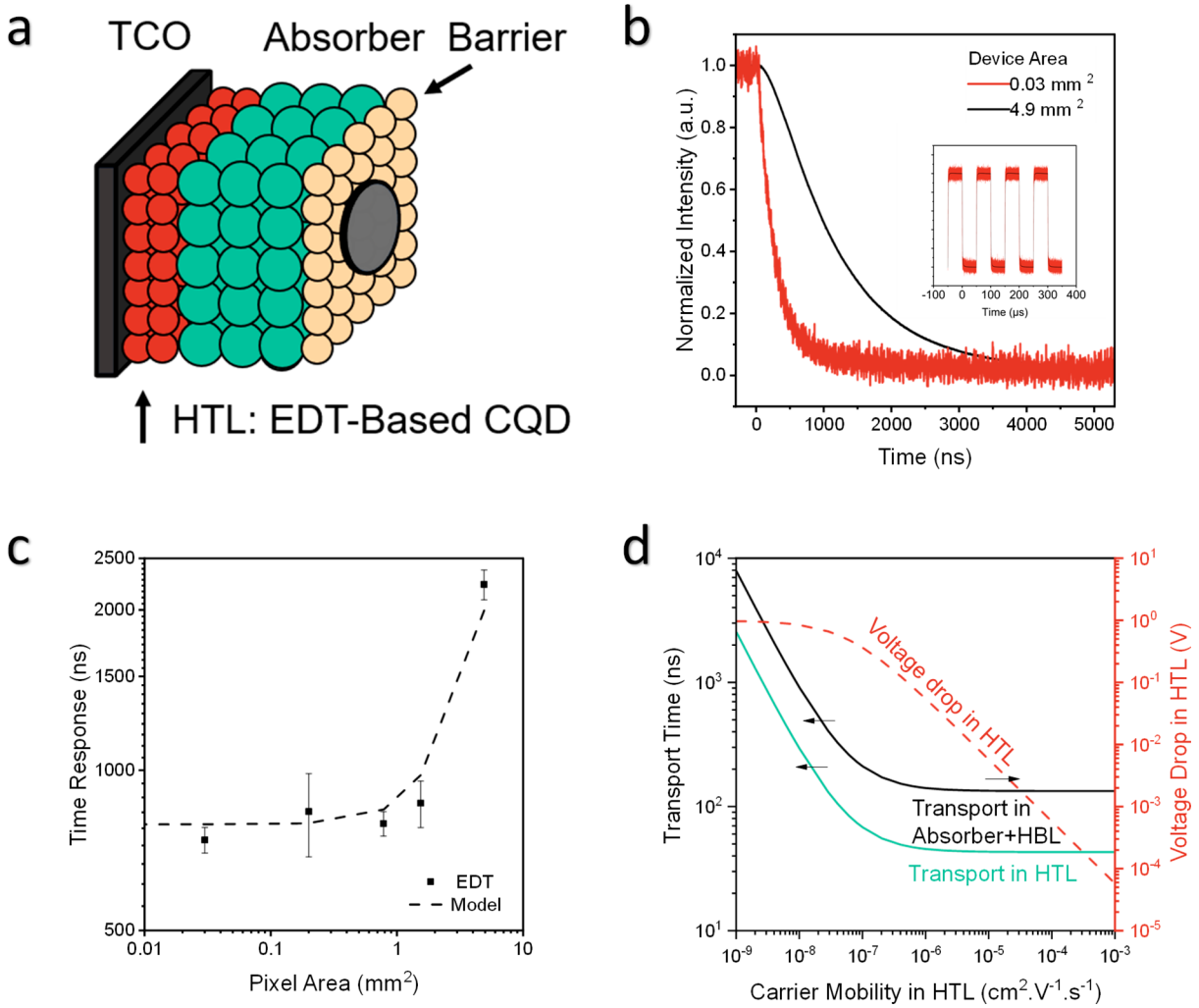

Figure 1. Characterization of reference devices. (a) Schematic of the device stack. TCO stands for transparent conducting oxide. (b) Temporal response of the reference structure illuminated with a 1310 nm laser modulated at 10 kHz with large and small active areas. The inset shows 4 ON−OFF cycles. (c) Fall time of the device with different active areas. (d) Voltage drop in HTL and transport time in device layers as a function of HTL mobility.

PbS CQDs were utilized in this work, one having an excitonic peak at 1350 nm and the other at 930 nm. Smaller CQDs were used for HTL and HBL deposition, while larger dots were used for the absorber layer. All dots were synthesized using previously published methods.[14] The PbS CQD-based HTL (bandgap ∼1.3 eV) is fabricated via solid state exchange where insulating oleic acid ligands are exchanged with EDT. The small size of the EDT ligand provides conductivity and p-type doping. The PbS CQD absorber layer and a hole-blocking layer (HBL) (used to block hole injection to the top contact) are fabricated using solution-phase exchange methods. For the absorber layer (bandgap ∼0.9 eV), a mixed halide exchange is used.[2] For the HBL, PbS CQDs (1.3 eV bandgap) exchanged with *trans*-4-(trifluoromethyl) cinnamic acid (TFCA) ligands are chosen, since these provide n-type behavior and increase the work function of the HBL, facilitating electron transport to the electrode.[3] The devices exhibit 50% EQE, 3×10^{-3} mA cm^{-2} dark current at 1 V reverse bias, and $\sim 10^3$ rectification ratio (Figure S1).

PbS CQD photodetectors with large active areas exhibit a response that is RC-limited. To move instead into the transport-limited regime, we created detectors with different active areas, ranging from 0.03 to 4.9 mm^2 (Figure 1b). We characterized these devices for detection speed based on the 90%−10% fall time of the response when illuminated using a modulated 1310 nm laser (pulse frequency is 10 kHz). The measurements were performed under 1 V reverse bias to ensure full depletion (Figure S9). We observed that the response time decreased as the active area decreased, reaching a plateau at ca. 1 mm^2, where the response time remained constant at approximately 800 ns (Figure 1c).

We sought to use a model to understand the factors limiting the temporal response of the photodetectors. The model uses the RC time constant (t_{RC}) and the charge carrier transit time (t_{tr}) for temporal response (see eq 2 in the Experimental Methods section in the Supporting Information). In this model, we neglected the diffusion time constant under an applied reverse bias, because under complete depletion conditions, the signal is dominated by drift current (Figure S9). The model predicts the measured fall time accurately (Figure 1c). The slow time response of large active-area devices is due to the RC time constant; below 1 mm^2, the photodetectors operate in the transport-limited regime where the response is independent of the active area.

https://doi.org/10.1021/acs.nanolett.3c00491
Nano Lett. XXXX, XXX, XXX−XXX

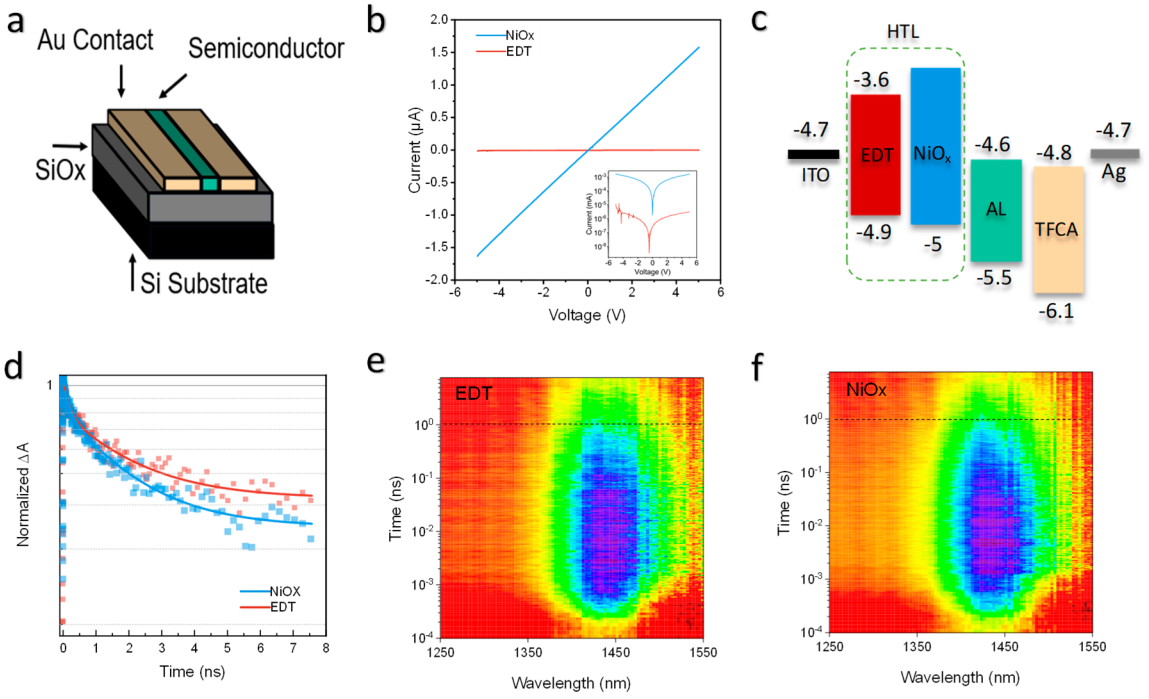

Figure 2. Characterization of NiOx and EDT. (a) Schematic of devices used for the conductivity study. (b) Conductivity study of NiOx and EDT: $I-V$ curves for the materials (with log scale in the inset). (c) Band diagram for the full device. AL stands for the absorber layer. (d) TA measurements on glass/ITO/NiOx/AL and glass/ITO/EDT/AL structures investigating charge carrier extraction dynamics. (e, f) 2D contour plots showing TA spectra of EDT and NiOx as a function of delay time between pump and the probe.

When we increase, in the model, the carrier mobility of the HTL, we see the potential to decrease the response time to ∼200 ns (Figure 1d); the increased carrier mobility reduces the resistance of the HTL, increasing the electric field within the absorber layer and reducing the transit time (Figure 1d). We estimate that, when we increase the mobility, the drift time through HTL improves 2 orders of magnitude for NiOx compared to EDT-capped PbS CQDs: specifically, it goes from ∼400 ns to a near-negligible ∼ns through the HTL. The transit time through the absorber layer is reduced (again, by increasing the electric field within the absorber layer) from ∼400 to ∼200 ns. The sum of these two transit times thus goes from ∼800 to ∼200 ns, accounting for the observed 4× decrease in total drift time (Table S1).

The EDT-passivated PbS CQD layer has been reported to have relatively low carrier mobility in the range of $10^{-5}-10^{-4}$ cm^2 V^{-1} s^{-1}.[15,16] To ascertain the magnitude of the carrier mobility of the PbS CQD HTL layer, we employed field-effect transistors (FETs) with a device structure as shown in Figure 2a. The transfer characteristics of the EDT FET showed a unipolar response with an I_{on}/I_{off} ratio of $\sim 10^3-10^4$ (Figure S3). The current saturation (pinch-off) region can be observed in the output curve, which indicates that the drain current becomes almost independent from the drain-source voltage (Figure S3). The resulting saturation mobility was estimated to be $(2-3) \times 10^{-5}$ cm^2 V^{-1} s^{-1}, consistent with prior reports.[17,18]

These findings motivated us to explore replacing the PbS CQD-based HTL with a metal oxide. We choose NiOx for its high carrier mobility, suitable band alignment with the PbS CQD in the active layer, and high stability.[19−22] Solution processed (sol−gel) NiOx HTL has been used with PbS CQD active layers in the past to achieve an EQE of 24% at 1 V reverse bias.[23] The reported valence band position of the sol−gel NiOx (5.4 eV) is deep and close to the valence band energy reported for the PbS CQD based absorber layer (5.2−5.5 eV[2,3]). This band alignment mismatch obstructs efficient charge extraction, leading to low EQE values. Further, sol−gel NiOx has lower conductivity (Figure S11) than sputtered NiOx. We therefore redirected our efforts to develop a radio frequency (RF) sputtering process to fabricate NiOx layers, targeting the desired band alignment and mobility. We deposited a NiOx layer having a thickness of 20 nm. The measured valence band maximum for RF sputtered NiOx is 5 eV compared to 5.3 eV for sol−gel NiOx. This enables increased band bending, leading to a larger built-in electric field with sputtered NiOx (Figure S12). We controlled the oxygen gas flow rate and chamber pressure during the sputtering process to optimize performance. We also optimized postdeposition annealing conditions for sputtered NiOx to obtain conductive and smooth films (Figures S7, S10, and S12). We characterized the conductivity of the NiOx layer and compared it to that of the EDT-based HTL. For this, we fabricated Ohmic devices where the HTL was sandwiched between an ITO and Au electrode and measured the $I-V$ characteristics in the dark (Figure 2b). The conductivity of NiOx was found to be 5×10^{-3} S cm^{-1}, compared to 1×10^{-5} S cm^{-1} in the case of EDT-CQDs.

We then verified whether the NiOx HTL is suitable for hole extraction in PbS CQD infrared photodetectors. Ultraviolet photoelectron spectroscopy (UPS) suggests that NiOx does not create a potential barrier for charge carriers (Figure 2c and Figure S6). Transient absorption (TA) measurements performed on ITO/HTL/absorber samples show similar decay times, indicating that NiOx can have similar efficiency in hole extraction as EDT (Figure 2d-f).

https://doi.org/10.1021/acs.nanolett.3c00491
Nano Lett. XXXX, XXX, XXX−XXX

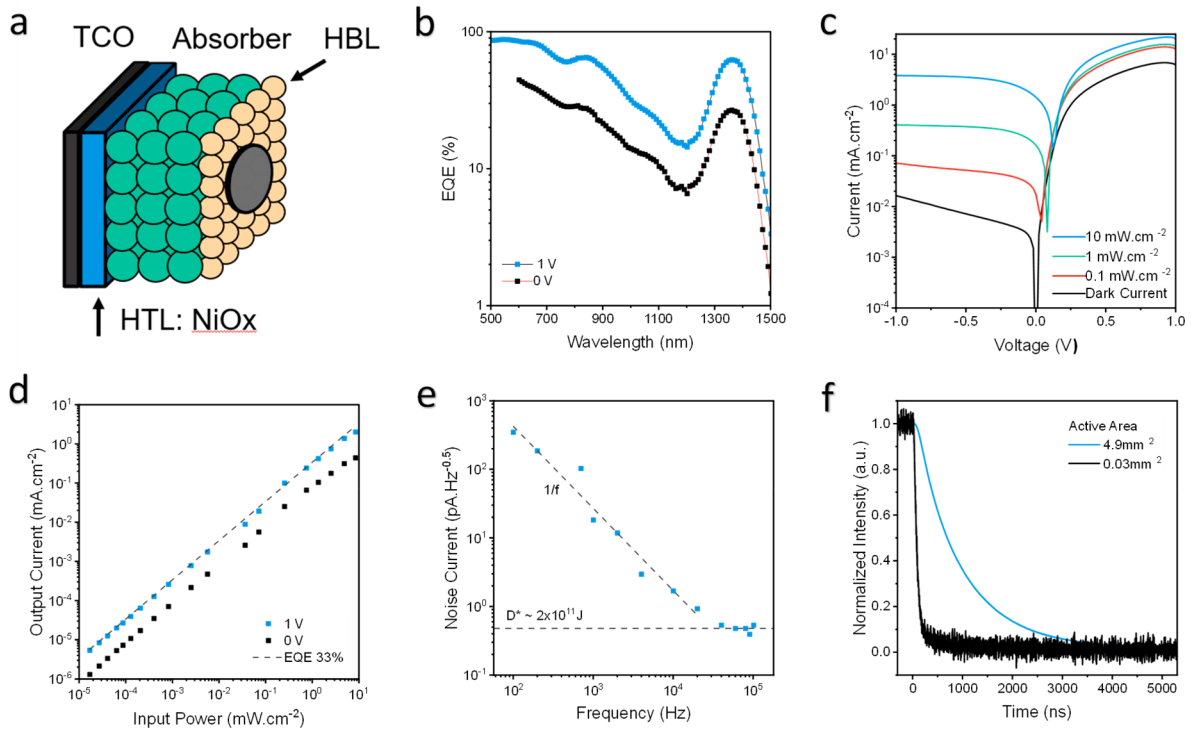

Figure 3. Integration and characterization of NiOx/PbS CQD devices. (a) Schematic of the fabricated devices. (b) EQE spectra (30% at 0 V and 65% at 1 V reverse bias). (c) Power-dependent $I-V$ curves of the device using laser excitation. (d) Dynamic range using 1310 nm laser excitation. (e) Dependence of noise current on frequency under short circuit conditions. (f) Temporal response of the control structure illuminated with a 1310 nm laser modulated at 10 kHz with large and small active areas.

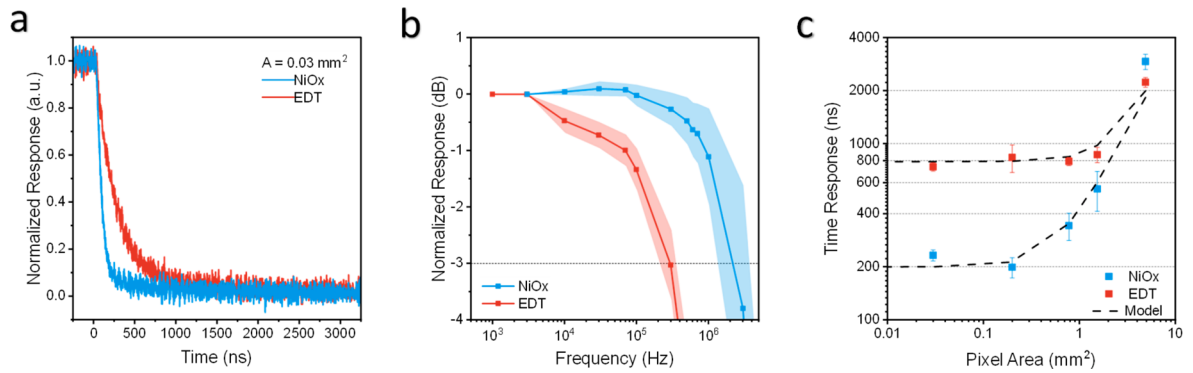

Figure 4. Experimental study of temporal response. (a) Temporal response comparison of small active area NiOx and EDT devices. (b) Bandwidth comparison of NiOx and EDT devices using 0.03 mm^2 pixels. (c) Fall time comparison of the NiOx and EDT devices with different active areas.

We fabricated photodetector devices operating at 1370 nm with NiOx as the HTL (Figure 3a). We used the same structure as for the EDT HTL device to enable a direct comparison of performance and assess the influence of the higher carrier mobility HTL on the response time. The resulting photodetector exhibited performance similar to that of the devices made with the EDT HTL, with an EQE of 65% under 1 V reverse bias at the excitonic peak position of 1370 nm (Figure 3b).

The NiOx HTL devices showed a linear photoresponse with respect to input power of over 6 orders of magnitude (Figure 3d). Responsivity was constant over the range of $10^{-5}-10$ mW cm^{-2} of input power (Figure S8). A linear relationship between input power and output current suggests low trap density in these devices.[24]

Photodetector noise was characterized at short circuit conditions under different operating frequencies. We observed different noise regimes: at low frequencies, flicker ($1/f$) noise is dominant, while at high frequencies, the response is limited by shot noise (Figure 3e). This behavior has been reported in PbS-CQD devices before.[2,25,26] We measured a specific detectivity reaching 2×10^{11} jones at the 1370 nm excitonic peak, which is in good agreement with other PbS-CQDs operating in this wavelength regime.[2,3,5]

Next, we studied the temporal response of the photodetectors with the NiOx HTL. The response time improved with a decrease in the active area (Figure 3f), as seen in the EDT case. The devices also showed a transition from the RC-limited regime to the transport-limited regime around an active area of 1 mm^2. In the transport-limited regime the NiOx-based

https://doi.org/10.1021/acs.nanolett.3c00491
Nano Lett. XXXX, XXX, XXX−XXX

devices exhibit a fall time of 200 ns, which is 4× faster than the response from the EDT devices (Figure 4a).

We measured the bandwidths of both NiOx and EDT devices, which are shown in Figure 4b. The 3 dB bandwidths are 300 kHz for the EDT devices and 1.5 MHz for the NiOx devices. This 5× improvement corresponds well to the reduction in response time.

The measured fall time values for both NiOx and EDT devices with respect to active area (mm^2) are summarized in Figure 4c. We observed the same trends for both devices as we moved from a large active area to a smaller active area. The theoretical values we used to model the temporal response of NiOx devices are given in Table S1. A comparison among fitted total resistance, calculated total resistance, expected time constants, and calculated drift times are shown in Tables S2–S5.

Overall, with NiOx, the transport through the HTL is no longer the speed-limiting factor. The speed of the photodetector is now limited not by the transport layer properties, but by those of the light-absorbing active layer.

In conclusion, we examined the origins of slow temporal response in prior CQD photodiodes. We find that the low mobility of the charge carriers in the HTL was limiting the photodiode speed of response. Replacing EDT-capped CQDs with NiOx increases the carrier mobility in the charge transport layers and increases the electric field within the absorber layer, increasing speed in photodiodes by 4×.

■ ASSOCIATED CONTENT

Supporting Information

The Supporting Information is available free of charge at https://pubs.acs.org/doi/10.1021/acs.nanolett.3c00491.

Detailed description of the synthesis and ligand exchanges, characterization of the reference devices, FET data, AFM and SEM images, UPS and XPS spectra, capacitance–voltage measurement for devices, device performance using NiOx deposited in oxygen-poor and oxygen-rich environments, tables summarizing physical and electronic parameters used for device simulations, and simulated drift time versus mobility data (PDF)

■ AUTHOR INFORMATION

Corresponding Author

Edward H. Sargent − *Department of Electrical and Computer Engineering, University of Toronto, Toronto, Ontario M5S 3G4, Canada;* orcid.org/0000-0003-0396-6495; Email: ted.sargent@utoronto.ca

Authors

Ozan Atan − *Department of Electrical and Computer Engineering, University of Toronto, Toronto, Ontario M5S 3G4, Canada;* orcid.org/0000-0003-1439-8470

Joao M. Pina − *Department of Electrical and Computer Engineering, University of Toronto, Toronto, Ontario M5S 3G4, Canada;* orcid.org/0000-0002-3448-0028

Darshan H. Parmar − *Department of Electrical and Computer Engineering, University of Toronto, Toronto, Ontario M5S 3G4, Canada;* orcid.org/0000-0001-9533-7594

Pan Xia − *Department of Electrical and Computer Engineering, University of Toronto, Toronto, Ontario M5S 3G4, Canada*

Yangning Zhang − *Department of Electrical and Computer Engineering, University of Toronto, Toronto, Ontario M5S 3G4, Canada*

Ahmet Gulsaran − *Waterloo Institute for Nanotechnology (WIN), University of Waterloo, Waterloo, Ontario N2L 3G1, Canada; Department of Mechanical and Mechatronics Engineering, University of Waterloo, Waterloo, Ontario N2L 3G1, Canada*

Eui Dae Jung − *Department of Electrical and Computer Engineering, University of Toronto, Toronto, Ontario M5S 3G4, Canada;* orcid.org/0000-0003-4848-0931

Dongsun Choi − *Department of Electrical and Computer Engineering, University of Toronto, Toronto, Ontario M5S 3G4, Canada*

Muhammad Imran − *Department of Electrical and Computer Engineering, University of Toronto, Toronto, Ontario M5S 3G4, Canada;* orcid.org/0000-0001-7091-6514

Mustafa Yavuz − *Waterloo Institute for Nanotechnology (WIN), University of Waterloo, Waterloo, Ontario N2L 3G1, Canada; Department of Mechanical and Mechatronics Engineering, University of Waterloo, Waterloo, Ontario N2L 3G1, Canada*

Sjoerd Hoogland − *Department of Electrical and Computer Engineering, University of Toronto, Toronto, Ontario M5S 3G4, Canada;* orcid.org/0000-0002-3099-585X

Complete contact information is available at: https://pubs.acs.org/10.1021/acs.nanolett.3c00491

Author Contributions

O.A., J.M.P., and D.H.P. contributed equally to this work.

Notes

The authors declare no competing financial interest.

■ ACKNOWLEDGMENTS

The authors thank L. Levina, E. Palmiano, R. Wolowiec, and D. Kopilovic for their technical assistance.

■ REFERENCES

(1) Hansen, M. P.; Malchow, D. S. Overview of SWIR detectors, cameras, and applications. *Proc. SPIE 6939, Thermosense* 2008, Vol. *6939*, p 94104

(2) Pina, J.; Vafaie, M.; Parmar, D.; Atan, O.; Xia, P.; Zhang, Y.; Najarian, A.; De Arquer, F.; Hoogland, S.; Sargent, E. Quantum-Size-Effect Tuning Enables Narrowband IR Photodetection with Low Sunlight Interference. *Nano Lett.* **2022**, *22* (16), 6802−6807.

(3) Zhang, Y.; Vafaie, M.; Xu, J.; Pina, J.; Xia, P.; Najarian, A.; Atan, O.; Imran, M.; Xie, K.; Hoogland, S.; Sargent. Electron-Transport Layers Employing Strongly Bound Ligands Enhance Stability in Colloidal Quantum Dot Infrared Photodetectors. *Adv. Mater.* **2022**, *34*, 2206884.

(4) Parmar, D. H.; Pina, J. M.; Zhu, T.; Vafaie, M.; Atan, O.; Biondi, M.; Najjariyan, A. M.; Hoogland, S.; Sargent, E. H. Controlled Crystal Plane Orientations in the ZnO Transport Layer Enable High-Responsivity, Low-Dark-Current Infrared Photodetectors. *Adv. Mater.* **2022**, *34* (17), 2200321.

(5) Vafaie, M.; Fan, J. Z.; Najarian, A. M.; Ouellette, O.; Sagar, L. K.; Bertens, K.; Sun, B.; Arquer, F. P. G. d.; Sargent, E. H. Colloidal quantum dot photodetectors with 10-ns response time and 80% quantum efficiency at 1,550 nm. *Matter* **2021**, *4* (3), 1042−1053.

(6) Baker, I.; Owton, D.; Trundle, K.; Thorne, P.; Storie, K.; Oakley, P.; Copley, J. Advanced infrared detectors for multimode active and passive imaging applications. In *Infrared Technology and Applications XXXIV*; SPIE: 2008.

(7) Rutz, F.; Kleinow, P.; Aidam, R.; Bronner, W.; Stolch, L.; Benecke, M.; Sieck, A.; Rehm, R. SWIR detectors for low photon fluxes. in *Infrared Sensors, Devices, and Applications VI*; SPIE: 2016.
(8) Hadji, B. Understanding wavelength choice in LiDAR systems. *EE Times*, 2021. [Online]. Available: https://www.embedded.com/understanding-wavelength-choice-in-lidar-systems/ (Accessed 01 February 2023.
(9) Gupta, M.; Yin, Q.; Nayar, S. Structured light in sunlight. in *Proceedings of the IEEE International Conference on Computer Vision*; IEEE: 2013; pp 545−552.
(10) Kazmi, W.; Foix, S.; Alenya, G. Plant leaf imaging using time of flight camera under sunlight, shadow and room conditions. In *2012 IEEE International Symposium on Robotic and Sensors Environments Proceedings*; IEEE: 2012; pp 192−197.
(11) Clifford, J. P.; Konstantatos, G.; Johnston, K. W.; Hoogland, S.; Levina, L.; Sargent, E. H. Fast, sensitive and spectrally tuneable colloidal-quantum-dot photodetectors. *Nature Nanotechnol.* **2009**, *4* (1), 40−44.
(12) Choi, M.-J.; Arquer, F. P. G. d.; Proppe, A. H.; Seifitokaldani, A.; Choi, J.; Kim, J.; al, S.-W. B. e. Cascade surface modification of colloidal quantum dot inks enables efficient bulk homojunction photovoltaics. *Nat. Commun.* **2020**, *11* (1), 1−9.
(13) Goossens, S.; Konstantatos, G.; Oikonomou, A. Colloidal Quantum Dot Image Sensors: Technology and Marketplace Opportunities. *Information Display* **2021**, *37* (6), 18−23.
(14) Hines, M. A.; Scholes, G. D. Colloidal PbS nanocrystals with size-tunable near-infrared emission: observation of post-synthesis self-narrowing of the particle size distribution. *Adv. Mater.* **2003**, *15* (21), 1844−1849.
(15) Biondi, M.; Choi, M.-J.; Wang, Z.; Wei, M.; Lee, S.; Choubisa, H.; Sagar, L. K.; Sun, B.; Baek, S.-W.; Chen, B.; Todorovic, P.; Najarian, A. M.; Sedighian Rasouli, A.; Nam, D.-H.; Vafaie, M.; Li, Y. C.; Bertens, K.; Hoogland, S.; Voznyy, O.; Garcia de Arquer, F. P.; Sargent, E. H. Facet-Oriented Coupling Enables Fast and Sensitive Colloidal Quantum Dot Photodetectors. *Adv. Mater.* **2021**, *33* (33), 2101056.
(16) Speirs, M. J.; Dirin, D. N.; Abdu-Aguye, M.; Balazs, D. M.; Kovalenko, M. V.; Loi, M. A. Temperature dependent behaviour of lead sulfide quantum dot solar cells and films. *Energy Environ. Sci.* **2016**, *9* (9), 2916−2924.
(17) Balazs, D. M.; Nugraha, M. I.; Bisri, S. Z.; Sytnyk, M.; Heiss, W.; Loi, M. A. Reducing charge trapping in PbS colloidal quantum dot solids. *Appl. Phys. Lett.* **2014**, *104* (11), 112104.
(18) Klem, E. J.; Shukla, H.; Hinds, S.; MacNeil, D. D.; Levina, L.; Sargent, E. H. Impact of dithiol treatment and air annealing on the conductivity, mobility, and hole density in PbS colloidal quantum dot solids. *Appl. Phys. Lett.* **2008**, *92* (21), 212105.
(19) Yang, M.; Pu, H.; Zhou, Q.; Zhang, Q. Transparent p-type conducting K-doped NiO films deposited by pulsed plasma deposition. *Thin Solid Films* **2012**, *520* (18), 5884−5888.
(20) Itapu, S.; Georgiev, D. G.; Uprety, P.; Podraza, N. J. Modification of reactively sputtered NiOx thin films b pulsed UV laser irradiation. *physica status solidi* **2017**, *214* (2), 1600414.
(21) Grilli, M. L.; Menchini, F.; Dikonimos, T.; Nunziante, P.; Pilloni, L.; Yilmaz, M.; Piegari, A.; Mittiga, A. Effect of growth parameters on the properties of RF-sputtered highly conductive and transparent p-type NiOx films. *Semicond. Sci. Technol.* **2016**, *31* (5), 055016.
(22) Chen, S.; Kuo, T.; Lin, Y.; Lin, H. Preparation and properties of p-type transparent conductive Cu-doped NiO films. *Thin Solid Films* **2011**, *519* (15), 4944−4947.
(23) Manders, J. R.; Lai, T.; An, Y.; Xu, W.; Lee, J.; Kim, D. Y.; Bosman, G.; So, F. Low-noise multispectral photodetectors made from all solution-processed inorganic semiconductors. *Adv. Funct. Mater.* **2014**, *24* (45), 7205−7210.
(24) Xu, Q.; Cheong, I. T.; Song, H.; Van, V.; Veinot, J. G.; Wang, X. Heterogeneous Integration of Colloidal Quantum Dot Inks on Silicon Enables Highly Efficient and Stable Infrared Photodetectors. *ACS Photonics* **2022**, *9* (8), 2792−2801.
(25) García de Arquer, F. P.; Gong, X.; Sabatini, R. P.; Liu, M.; Kim, G.-H.; Sutherland, B. R.; al, O. V. e.; et al. Field-emission from quantum-dot-in-perovskite solids. *Nat. Commun.* **2017**, *8* (1), 1−8.
(26) Liu, H.; Lhuillier, E.; Guyot-Sionnest, P. 1/f noise in semiconductor and metal nanocrystal solids. *J. Appl. Phys.* **2014**, *115* (15), 154309.

https://doi.org/10.1021/acs.nanolett.3c00491
Nano Lett. XXXX, XXX, XXX−XXX